Growth and Oxidation of Ni Nanostructures on Stepped Rh Surfaces

ARTICLE *in* THE JOURNAL OF PHYSICAL CHEMISTRY C · DECEMBER 2008

Impact Factor: 4.77 · DOI: 10.1021/jp807259n

Article

Growth and Oxidation of Ni Nanostructures on Stepped Rh Surfaces

G. Parteder, F. Allegretti, M. Wagner, M. G. Ramsey, S. Surnev, and F. P. Netzer

J. Phys. Chem. C, **2008**, 112 (49), 19272-19278 • Publication Date (Web): 12 November 2008

Growth and Oxidation of Ni Nanostructures on Stepped Rh Surfaces

G. Parteder, F. Allegretti,* M. Wagner, M. G. Ramsey, S. Surnev, and F. P. Netzer

Institute of Physics, Surface and Interface Physics, Karl-Franzens Universität Graz, A-8010 Graz, Austria

Received: August 14, 2008; Revised Manuscript Received: September 19, 2008

The growth and oxidation of Ni nanostructures on stepped Rh(15 15 13) and (553) surfaces, both vicinals of Rh(111), have been studied by scanning tunneling microscopy (STM), LEED, core level spectroscopies with use of synchrotron radiation (XPS and NEXAFS), and work function measurements. At low coverages, quasi-one-dimensional Ni rows decorate the Rh step edges. With increasing coverages, the Ni adlayers grow layer-by-layer in a restricted step-flow growth mode, pseudomorphically up to ~2 monolayer (ML). Relaxation to the Ni bulk lattice occurs in the range 2−10 ML. The oxidation of the low-coverage Ni nanowires creates ordered quasi-one-dimensional Ni−O structures at the Rh step edges. In the Ni coverage range up to 2 ML, uniaxially ordered (2 × 1) and (6 × 1) oxide structures are observed. On thicker films, local NiO (100)-type and (111)-type reconstructions are both observed in the STM. The NEXAFS measurements indicate that the low-dimensional Ni−O nanophases are distinctly different from bulk-type NiO, and three chemically different oxygen species are identified in the O 1s XPS core level spectra. The chemical reactivity of the Ni−Rh surfaces toward oxygen seems to be highest for the one-dimensional Ni−Rh nanowires, where the Ni atoms are coupled directly with the Rh step atoms.

1. Introduction

The combination of two metals at a surface has been recognized as a very successful concept in heterogeneous catalysis. The unique chemical properties of these so-called bimetallic catalysts in terms of superior reactivity and selectivity as compared to their single component counterparts have been ascribed to geometric (ensemble) and/or electronic (ligand) effects.[1−3] Surface systems with controlled morphology containing bimetallic aspects may be found at the surfaces of bulk alloys or may be generated by covering a single crystal surface of one metal by a thin layer of another metal. In the latter case, suitable temperature treatments result in the creation of surface alloy phases with well-defined geometry and atomic distribution.[4] In the present work, we were interested in another modification of a metal surface with bimetallic character, namely decorating it with nanostructures of a second metal. Using the regular, monatomic step array of a vicinal surface as a nanoscale template, we have studied the growth of Ni nanostructures on the (15 15 13) and (553) surfaces of rhodium, both vicinals of Rh(111). The morphology and chemical reactivity of a bimetallic system may be changed by oxidation.[5] Here we have oxidized the Ni nanostructures on the stepped Rh surfaces to create low-dimensional Ni-oxide nanostructures. The latter are not only of interest from a catalytic chemical point of view but also for magnetic purposes: bulk NiO is an antiferromagnet, but the magnetic properties of low-dimensional NiO_x phases are largely unexplored.

Recently, we have reported succinctly that Ni adatoms at low coverages can be self-assembled into quasi-one-dimensional nanowires on vicinal Rh(111) surfaces by decorating their regular step arrays.[6] These bimetallic Ni−Rh nanowires have specific electronic properties that lead to a significantly enhanced chemical reactivity toward oxygen.[7] As a result, the Ni−Rh nanowires can be oxidized preferentially, generating novel quasi-one-dimensional (quasi-1D) oxide structures.[7] In the present paper we give a full account of this work and present the growth properties and the oxidation of Ni overlayers on Rh(15 15 13) and Rh(553) surfaces from low Ni coverages up to several monolayer thick Ni films. We have used scanning tunneling microscopy (STM) and low-energy electron diffraction (LEED) to determine growth morphology and structure, X-ray photoelectron spectroscopy (XPS) and near-edge X-ray absorption fine structure (NEXAFS) with use of synchrotron radiation to characterize adsorbate and oxide species and the oxidation kinetics, and laboratory-source UV photoelectron spectroscopy (UPS) to probe the valence states and the surface work function. The chemical properties of the surfaces prepared here have been also tested in terms of their reactivity for the oxidation reaction of CO, but this will be treated in a forthcoming publication.

Both vicinal Rh surfaces employed in this study expose (111) terraces separated by (111)-type microfacet step edges, the terrace widths being ~33.5 Å and ~10.4 Å for the (15 15 13) and (553) surfaces, respectively. The Rh(15 15 13) surface has been investigated in the STM measurements because more stable tunneling conditions could be obtained on the larger terraces, while the Rh(553) surface, which has the higher step density, has been probed by the spectroscopy techniques to enhance the step-derived effects in the spectra. LEED provided a common link between the measurements on the two surfaces. As expected, certain long-range growth effects are different on the two surfaces, but the local properties such as the reactivity toward oxygen were found to be quite comparable as discussed below.

2. Experimental Section

The experiments have been carried out in three different UHV systems with typical base pressures ~$1-2 \times 10^{-10}$ mbar. The STM experiments have been performed in a custom-designed variable-temperature STM system as described previously.[8] All STM images presented here have been recorded at room temperature and in constant-current mode. XPS and NEXAFS spectra have been measured at beamline I311 in the Swedish

* Corresponding author. Email: francesco.allegretti@uni-graz.at.

10.1021/jp807259n CCC: $40.75
Published on Web 11/12/2008

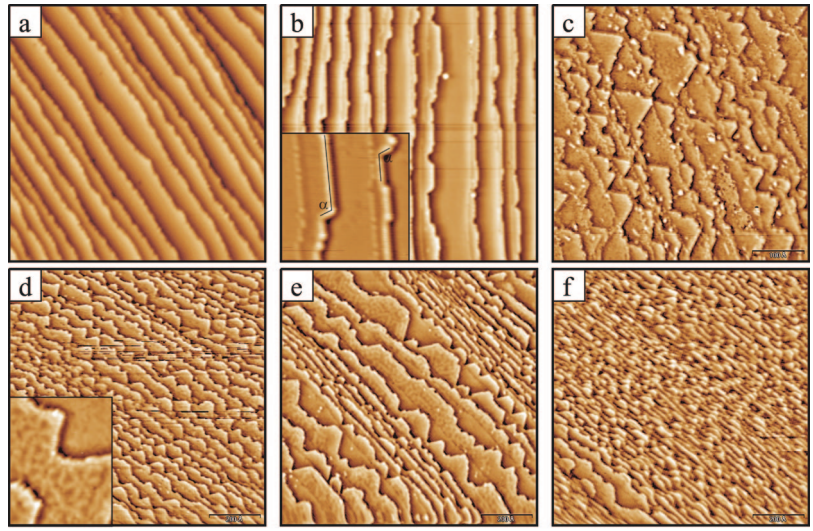

Figure 1. STM images of clean and Ni-covered Rh(15 15 13) surfaces: (a) clean (540 Å × 540 Å; sample bias $U = +2.0$ V; tunneling current $I = 0.3$ nA). (b) 0.25 ML Ni (500 Å × 500 Å; $U = +0.75$ V; $I = 0.2$ nA. Inset: 82 Å × 82 Å; $U = +0.75$ V; $I = 0.2$ nA). (c) 0.4 ML Ni (500 Å × 500 Å; $U = +0.5$ V; $I = 0.2$ nA). (d) 0.6 ML Ni (1000 Å × 1000 Å; $U = +1.0$ V, $I = 0.1$ nA. Inset: 174 Å × 216 Å; $U = +0.35$ V; $I = 0.1$ nA). (e) 0.8 ML Ni (1000 Å × 1000 Å; $U = +0.8$ V; $I = 0.1$ nA). (f) 1.0 ML Ni (1000 Å × 1000 Å; $U = +1.0$ V, $I = 0.1$ nA).

synchrotron radiation laboratory MAX-Lab, University of Lund, Sweden; the beamline and the electron spectrometer end station have been specified in ref 9; the total energy resolution in the present experiments was ∼100−200 meV. The NEXAFS spectrum of a thick NiO(100) layer (shown for comparison below in Figure 8) has been recorded at beamline BACH at the ELETTRA synchrotron, Trieste. The energy resolution here was also better than 200 meV in the respective photon energy region. UPS and work function measurements were performed in an angle-resolving UV photoelectron spectrometer using He I resonance radiation.[10] The sample work function was determined from the low-energy secondary electron cutoff in UPS with a small negative sample bias (several volts). All systems contained LEED, sample surface cleaning facilities, and instrumentation for controlled physical vapor deposition (e-beam evaporators, quartz microbalances).

The vicinal Rh surfaces have been cleaned by heating in oxygen and by cycles of Ar ion bombardment and annealing. The preparation of a well-ordered Rh(15 15 13) surface with a regular step array is difficult because the interaction between steps across the wide terraces, which provides the basis for the regular step arrangement, is weak. A typical STM image of the clean Rh(15 15 13) surface is shown in Figure 1a; the step edges are not particularly straight and the terraces display some variation of width. However, an autocorrelation analysis of the STM image gives a mean terrace width of ∼33 Å, which is close to the theoretical value. Nickel has been deposited from e-beam evaporators with typical evaporation rates of a few tenths of a monolayer per minute as measured by quartz microbalances (one monolayer is defined by the number of surface atoms on the Rh(111) surface). Oxygen has been introduced into the systems via leak valves, and typical oxygen pressures for oxidation were 1×10^{-7} to 5×10^{-8} mbar; the oxygen exposures are given in Langmuir ($1\ \text{L} = 1 \times 10^{-6}$ torr s).

3. Results and Discussion

3.1. The Growth of Ni Nanostructures on Stepped Rh Surfaces. Figure 1 displays STM images of the clean Rh(15 15 13) surface (a) and after deposition of various amounts of Ni at 150 °C substrate temperature (b−f). In Figure 1b the surface has been covered by 0.25 ML Ni. As reported previously,[6] under these conditions the Ni adatoms decorate the bottom of the Rh step edges with one-to-several-atom-wide rows in a nearly perfect way, forming Ni nanowires coupled to the Rh step atoms; no Ni adatoms or ad-islands are seen on the Rh terraces. It is noted that the Ni-decorated surface has straighter step edges than the bare Rh surface. The zoom-in image of the inset of Figure 1b shows that the Ni atoms appear bright owing to chemical contrast and that the Rh step edges can also be recognized. From the detailed analysis of the widths of the Ni stripes and the angles at the kinks it has been concluded that the Ni rows grow pseudomorphically with the Rh surface lattice. This conclusion has been supported by density functional theory (DFT) calculations, which indicated that the formation of pseudomorphic Ni rows, even with a 9% strained lattice, is energetically favorable.[6] Notably, there is no propensity of surface alloy formation for Ni on stepped Rh surfaces, in contrast to what has been reported for the growth of Ni on vicinal Pt surfaces.[11]

Figure 1c shows an STM image of the Rh(15 15 13) surface covered with 0.4 ML Ni. Here the Ni deposits display a drastically changed morphology, with triangular two-dimensional (2D) monolayer island structures extending from the lower step edges into the terrace areas. This morphology is in contrast to the DFT calculations,[6] which predicted a row-by-row decoration of the step edges also for increasing Ni coverages. However, the shapes of the Ni islands suggest that kinetic effects are at the root of this growth behavior: the triangular island structures may be the result of a 1D Schwoebel-type diffusion barrier around the kink edges of the Ni stripes. The 2D Ni triangles grow with their sides inclined by 60° (or 120°) with respect to the Rh step edges. If the diffusion of Ni adatoms at the edges of the 1D Ni stripes is restricted around kink sites (see Figure 1b, inset), islands will grow in the form of triangular shapes as indeed observed in Figure 1c. This process may be regarded as a particular kind of restricted step-flow growth mechanism.

The triangular island growth mode continues for higher coverages; see Figure 1d for 0.6 ML Ni. At this point, the Ni islands start to display dislocation lines on their surfaces (Figure 1d, inset). These are the result of the strain in the Ni overlayer owing to the pseudomorphic lattice growth. The dislocation

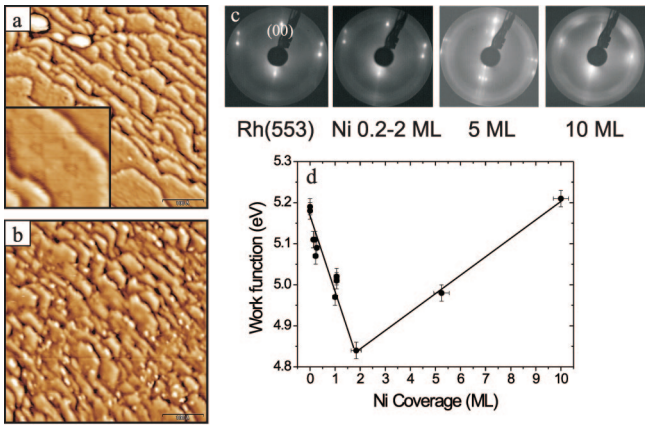

Figure 2. STM images of (a) 2 ML Ni (500 Å × 500 Å; $U = +0.35$ V; $I = 0.2$ nA) and (b) 5 ML Ni (500 Å × 500 Å; $U = +0.5$ V; $I = 0.1$ nA). The inset of (a) is 130 Å × 130 Å, with $U = +0.35$ V and $I = 0.2$ nA. (c) LEED patterns of clean Rh(553) ($E = 88$ eV), 0.2−2 ML Ni ($E = 88$ eV), 5 ML Ni ($E = 63$ eV), and 10 ML Ni ($E = 120$ eV). (d) Work function of Rh(553) versus Ni coverage.

pattern is clearly visible in the STM image of Figure 1e, at 0.8 ML Ni coverage. After 1 ML Ni deposition, Figure 1f, the surface is fully covered with a 2D Ni monolayer. The step pattern of the Rh template is still preserved, but the triangular 2D island growth mode results in a scalelike morphology with Ni monolayer platelets.

Figure 2 contains a collection of data of Ni growth from both Rh(15 15 13) and Rh(553) surfaces. The STM images of Figure 2a and 2b are representative of 2 and 5 ML Ni coverages on Rh(15 15 13), respectively. As seen, the step structure of the vicinal Rh surface is maintained at least up to 5 ML thick Ni films, indicating a layer-by-layer growth mode. On the 2 ML Ni surface a different dislocation pattern is recognized on the larger terraces: the inset of Figure 2a shows a hexagonal-like superlattice of triangular dislocations with a lattice constant of ∼30 Å. In Figure 2c a series of LEED patterns obtained from the Rh(553) surface is displayed. For Ni coverages up to 2 ML, the LEED patterns remain virtually identical to the one from the bare Rh(553) surface, confirming the pseudomorphic growth mode. At 5 ML Ni, spot splitting parallel to the Rh step edges can be observed, which suggests some long-range periodicity along the terraces. The LEED pattern from the 10 ML thick Ni film shows weak diffraction satellites around the diffuse integral order spots that may be associated with the presence of a Moiré-type interference pattern. Taken together, the LEED results may be considered as an indication that the Ni overlayer relaxes to its bulk lattice between 5 and 10 ML film thickness. The work function measurements from the Rh(553) surface in Figure 2d add further information on the Ni growth process. The work function of the clean Rh(553) surface (∼5.18 eV) decreases monotonically upon Ni deposition (at 150 °C) and reaches a minimum for 2 ML Ni at ∼4.86 eV. It increases again thereafter and reaches a value of ∼5.22 eV for the 10 ML film, which is close to the reported value in the literature for Ni(111) surfaces.[12,13]It is tempting to associate the work function minimum around 2 ML Ni coverage with the onset of transition from pseudomorphic to relaxed overlayer growth. The growth of the expanded pseudomorphic Ni layer leads to a decrease of the work function of Rh, but upon relaxation the lattice constant of the Ni overlayer decreases from 2.69 Å (a_{Rh}) to 2.49 Å (a_{Ni}), and the atomic density thus increases and the work function increases concomitantly.

To summarize briefly, Ni nanostructures decorate the step edges of vicinal Rh(111) surfaces under suitable kinetic conditions with quasi-1D atomic wires up to a coverage of ∼0.3 ML, but the presence of a 1D Schwoebel-type kink edge diffusion barrier precludes further row-by-row growth. 2D triangular Ni island structures attached with one side to the Rh step edges and extending into the terraces develop in a restricted step-flow growth mode. Further growth follows essentially a layer-by-layer process, at least up to 5 ML. The Ni overlayer up to ∼2 ML forms a pseudomorphic lattice, which relaxes to the Ni bulk lattice between 2 and 10 ML; the staircase step morphology of the substrate is maintained at the surface at least up to Ni coverages of 5 ML.

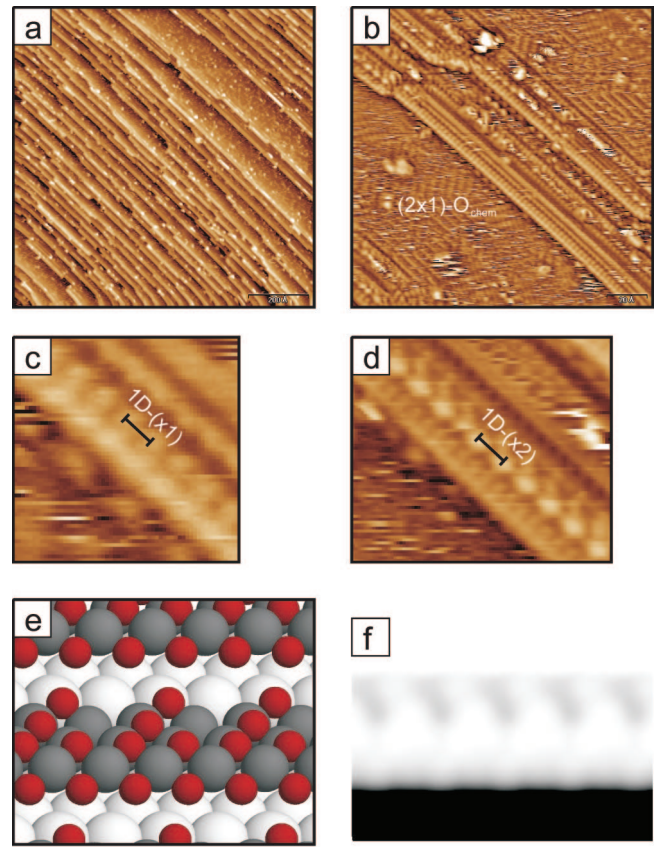

Figure 3. STM images of 0.3 ML Ni on Rh(15 15 13) exposed to 15 L O_2 at 300 °C: (a) 1000 Å × 1000 Å, $U = +1.0$ V, $I = 0.1$ nA. (b) 150Å × 150Å, $U = +0.13$ V, $I = 1.0$ nA. The chemisorbed oxygen areas on the Rh(111) terraces are indicated as (2 × 1)-O_{chem}. (c) 18 Å × 18 Å, $U = +0.13$ V, $I = 1.0$ nA. (d) 45Å × 37Å, $U = +0.14$ V, $I = 1.0$ nA. In (c) and (d) the periodicity along the steps is indicated as 1D-(×1) and 1D-(×2), respectively. (e) DFT model of a 0.6 ML Ni-oxide on Rh(553) and (e) corresponding simulated STM image.

3.2. The Oxidation of Ni Nanostructures on Stepped Rh Surfaces. The oxidation of bimetallic Ni−Rh nanostructures provides a suitable procedure for the fabrication of oxide−metal hybrid systems. As reported recently, 1D Ni−O line structures can be generated by the oxidation of Ni nanowires on stepped Rh surfaces.[7] Figure 3 shows STM images of the 0.3 ML Ni/Rh(15 15 13) surface after exposure to 15 L O_2 at 300 °C. Images 3a and 3b show straight step edges decorated by bright lines of protrusions, which display a linear 1D-(×1) and 1D-(×2) periodicity in terms of the Rh lattice constant parallel to the step edges (see Figure 3c and 3d). On the terrace areas, domains of a (2 × 1) structure of chemisorbed oxygen can be recognized. The oxygen-induced structures at the step edges are compatible with the DFT model of Mittendorfer et al.,[7] which is reproduced in Figure 3e for a 0.6 ML Ni-decorated Rh(553) surface (this decoration coverage corresponds roughly

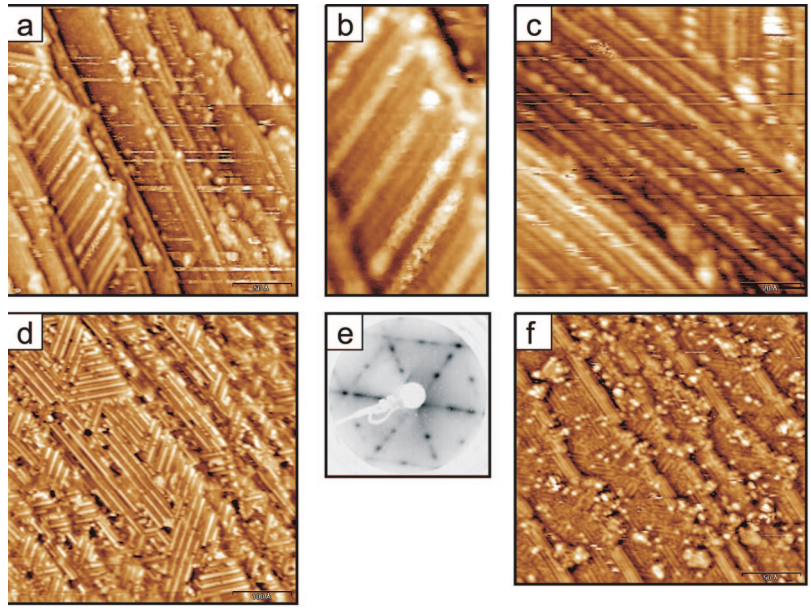

Figure 4. STM images of 0.4−1 ML Ni−O phases on Rh(15 15 13): (a) 0.4 ML Ni oxidized (250 Å × 250 Å; $U = +1.0$ V; $I = 0.1$ nA); (b) 0.4 ML Ni oxidized (96 Å × 53 Å; $U = +1.0$ V; $I = 0.1$ nA); (c) 0.6 ML Ni oxidized (100 Å × 100 Å; $U = +0.13$ V; $I = 0.2$ nA); (d) 0.8 ML Ni oxidized (500 Å × 500 Å; $U = +0.5$ V; $I = 0.1$ nA); (e) LEED pattern ($E = 50$ eV) corresponding to the surface of (d); (f) 1.0 ML Ni oxidized (250 Å × 250 Å; $U = +0.5$ V; $I = 0.1$ nA).

to the 0.3 ML Ni on Rh(15 15 13)). Accordingly, the Ni atoms in the first row at the step edges are coordinated to four O atoms each, forming a 1D-(×1) arrangement at the upper and lower step edge. Additional O adatoms are adsorbed in a (2 × 1) lattice on the other Ni rows, yielding the 1D-(×2) lines of bright maxima in the STM images. Formally, the overall stoichiometry of the Ni−O stripes corresponds to NiO. However, this formal stoichiometry has no relation to bulk NiO, since a fraction of the O atoms are shared between Ni and Rh surface atoms (in Figure 3e these are 50%, but this value depends on the widths of the Ni stripes). The NEXAFS spectra (see below) also confirm clearly that this Ni−O phase is different from NiO. It is also noticed that the O distribution is not uniform, because the Ni step edges are oxygen rich. This may have interesting consequences for the chemical reactivity of these Ni−O−Rh hybrid structures (as discussed in a forthcoming publication for the oxidation reaction of CO). The DFT simulations of STM images based on the model of Figure 3e revealed that the twofold periodicity of O atoms along the Ni stripes gives rise to the bright lines of maxima with twice the substrate periodicity (Figure 3f),[7] as seen in the experimental data (see Figure 3d). Similar 1D-(×2) periodicity has been observed in LEED for chemisorbed oxygen overlayers on vicinal Ni(111) surfaces and has been associated with a particular step-stabilized adsorbate phase.[14]

For larger Ni coverages the triangular 2D Ni islands become oxidized, and apart from the Ni−O structures at the step edges bright lines of protrusions are seen following the Ni island edges, running at 60° angles from the step edges into the terrace areas (Figure 4a). These lines correspond to (6 × 1) and (2 × 1) structures (Figure 4b and 4c), occurring in three domains and often coexistent at the surface. The latter is recognized best in Figure 4d for 0.8 ML Ni/Rh(15 15 13) exposed to 15 L O_2 at 300 °C. The LEED pattern from this surface (Figure 4e) confirms the (6 × 1) and (2 × 1) superstructures deduced from the STM images. These structures are also seen for 1 ML Ni coverage (Figure 4f). Figure 5 shows STM images of 2 ML (a, b) and 5 ML Ni (c, d) on Rh(15 15 13) after treatment with 15 L O_2 at 300 °C. This procedure is probably insufficient to fully

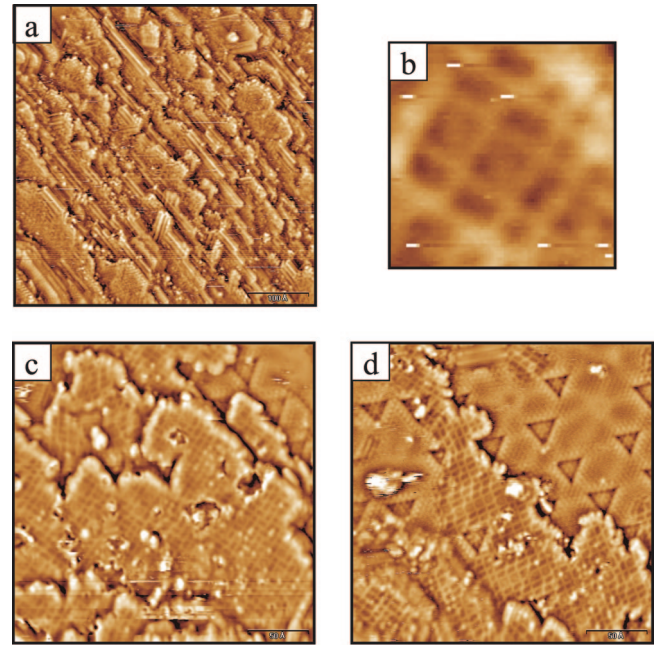

Figure 5. STM images of 2 ML (a, b) and 5 ML (c, d) Ni−O on Rh(15 15 13): (a) 500 Å × 500 Å with $U = +0.36$ V and $I = 0.1$ nA; (b) 9 Å × 9 Å with $U = +0.4$ V and $I = 0.1$ nA; (c) 250 Å × 250 Å with $U = +0.47$ V and $I = 0.2$ nA; (d) 250 Å × 250 Å with $U = +0.4$ V and $I = 0.1$ nA.

oxidize the thicker Ni films, but the 2 ML Ni surface still shows the (6 × 1) and (2 × 1) line structures, which are not recognized any more for 5 ML Ni. In addition, regions with square and rectangular lattice networks are apparent (see Figure 5b−d). These regions display only limited long-range order, but a detailed analysis of the network gives frequent distances of ~6 Å and ~8.8−9 Å. These distances are compatible with (2 × 2), (2 × 3), and (3 × 3) reconstructions of NiO(100), which have been also seen by Hildebrandt et al. [15] during the initial stages of oxidation of Ni(111) and have been interpreted in terms of NiO(100)-based (2 × 2), (2 × 3), and (3 × 3) cells. The

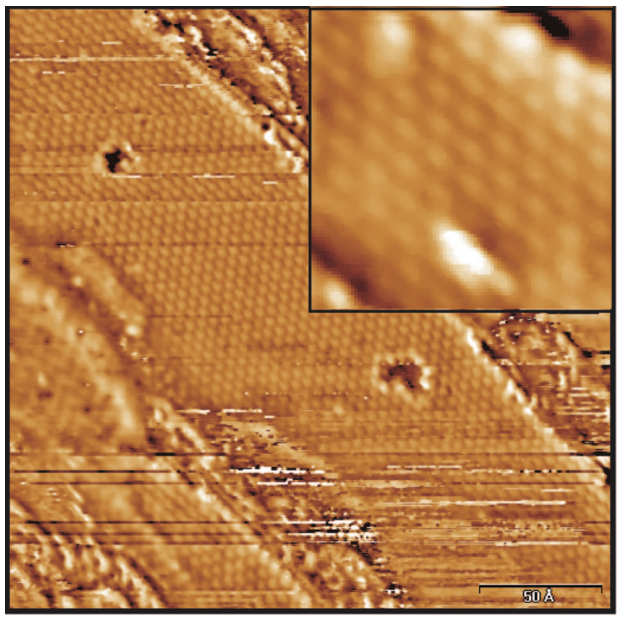

Figure 6. STM image of 2 ML Ni−O on Rh(15 15 13) (250 Å × 250 Å; $U = +0.32$ V; $I = 0.1$ nA). Inset: 30 Å × 30 Å; $U = +0.32$ V; $I = 0.1$ nA.

networks in the STM image of Figure 5 are remarkably similar to the STM images observed by Hildebrandt et al.[15] Our data thus indicate that NiO(100)-type surface phases nucleate locally during the initial oxidation of Ni layers on vicinal Rh(111) surfaces for films of 2 ML or thicker. NiO(001)-like arrangements have also been observed during the oxidation of Ni layers on Pt(111) at higher Ni coverages.[16]

In addition to the line structures and square/rectangular networks, local regions of hexagonal (2 × 2) and ($\sqrt{3} \times \sqrt{3}$)R30° reconstructions have been found on the surfaces of the oxidized Ni layers. These observations suggest that NiO(111)-type reconstructions form as well, as also observed for the Ni−O phases on the Pt(111) substrate.[16] Figure 6 shows STM images of a 2 ML Ni/Rh(15 15 13) surface after exposure to 9 L O_2 at 300 °C: a well-ordered (2 × 2) structure on a large terrace is recognized. The latter is of interest, since it is the dominant surface structure formed for ≥2 ML Ni−O overlayers on the flat Rh(111) surface;[17] it corresponds presumably to the octopolar (2 × 2) reconstruction of NiO(111)[18,19] and is presently the subject of further structure investigation. We note parenthetically that the (6 × 1) reconstruction of above has also been found after oxidation of 1 ML Ni on flat Rh(111).[17]

Although little differences in the reactivity toward oxygen are expected between Ni-decorated Rh(15 15 13) and Rh(553) surfaces (see below), the Ni−O surface structures formed on the two surfaces differ in some detail. In particular, the (6 × 1) superstructure is not detected on the Ni−O/Rh(553) surfaces; instead only (2 × 1) structures are observed, and for higher Ni coverages (>2 ML) also the (2 × 2) reconstruction is seen in the LEED patterns.[20] This is presumably due to the small terrace width of the (553) surface, which does not support the larger superstructure cells. The work function change of the 0.2 ML Ni/Rh(553) surface has been measured upon oxygen exposure at 300 °C: the work function increases by about 1 eV up to saturation (∼10 L),[20] as expected from the structure of Figure 3e and the electronegative nature of the oxygen adatoms.

The Ni−O nanostructures on Rh(553) have been characterized further by core level spectroscopies. Figure 7a shows XPS O 1s core level spectra of Rh(553) surfaces, decorated with increasing coverages of Ni up to 1.2 ML, exposed to saturation amounts of oxygen at $10^{-8}-10^{-7}$ mbar (typically 15−30 L) at 300 °C. For comparison, the spectrum of the bare Rh(553) surface exposed to 50 L O_2 at room temperature is included in Figure 7a, bottom curve. This latter spectrum consists of a single peak at 529.7 eV binding energy, labeled O, which is due to chemisorbed oxygen on Rh (for the purpose of this discussion, we refrain from a more detailed peak decomposition analysis, separating step and terrace contributions in this O 1s structure). On the 0.17 ML Ni-decorated Rh(553) surface, clearly two spectral components can be recognized in the O 1s emission: a larger peak at 528.9 eV (A) and a second component at 529.7 eV binding energy, which is due to the chemisorbed oxygen on the free Rh terraces (O). In our previous work on Ni−O nanowires on Rh(553), the O 1s emission at 528.9 eV (A) has been ascribed to the oxygen atoms coordinating the Ni step edges on the basis of DFT calculations.[7] The component A reaches a maximum intensity around the Ni coverage of 0.2 ML (curve A in Figure 7b): this is where under ideal conditions the Rh steps are decorated with single-atom Ni rows. The intensity of A then drops slowly with increasing Ni coverage, where it appears that full coordination of Ni step atoms by four O atoms is not realized any more. Possibly, repulsive interactions with O atoms chemisorbed on Ni come into play. The chemisorbed oxygen component vanishes above 0.24 ML (see curve O in Figure 7b), since free Rh terrace sites, in particular in connection with the (2 × 1)-O structure, become scarce. Instead, a new core-level component with a binding energy of 529.3 eV (B) appears, which grows in intensity with the increase of the Ni coverage. The increase of B as a function of Ni coverage suggests that O atoms chemisorbed on top of the Ni rows contribute to this component. From intermediate Ni coverages on, a third component (C) with a binding energy of 529.9 eV develops and increases in intensity. It is naturally associated with emission from oxygen atoms coordinated to Ni atoms as well. This emission occurs at a very similar binding energy as the O component of the chemisorbed oxygen on Rh. We notice also that, while component B saturates at ∼1 ML Ni coverage, component C apparently does not saturate. Figure 7c displays a set of O 1s spectra of 1 ML Ni−O on Rh(553) recorded at normal emission as a function of the photon energy. The three spectral components A, B, and C vary significantly in their relative intensities: this is due to photoelectron diffraction effects and indicates that A, B, and C are independent components associated with chemically different environments. The fact that structure C increases in intensity in going from 1 to 2.1 ML Ni−O suggests that C may be associated with oxygen atoms incorporated into the Ni layer, including coordination at the Ni−Rh interface.

Summarizing thus briefly, the O 1s XPS data give evidence of three distinctly different oxygen species on the Ni−O nanostructures. While the spectral component A at 528.9 eV binding energy is associated with O atoms bonded to Ni step atoms, components B (529.3 eV) and C (529.9 eV) are likely to be due to oxygen atoms at the surface of Ni terrace atoms and incorporated into the Ni layer, respectively; the latter are possibly coordinated to the Ni−Rh interface.

The near-edge fine structure in the X-ray absorption spectra is a sensitive probe of the local electronic structure of metal−oxygen coordination spheres.[21] The Ni 2p NEXAFS spectra of the Ni−O nanostructures on Rh(553) have been measured for Ni coverages from 0.2 to 1 ML. The NEXAFS profiles are very similar for the various Ni−O coverages in this range, and Figure 8 shows, by way of example, the Ni 2p (L-

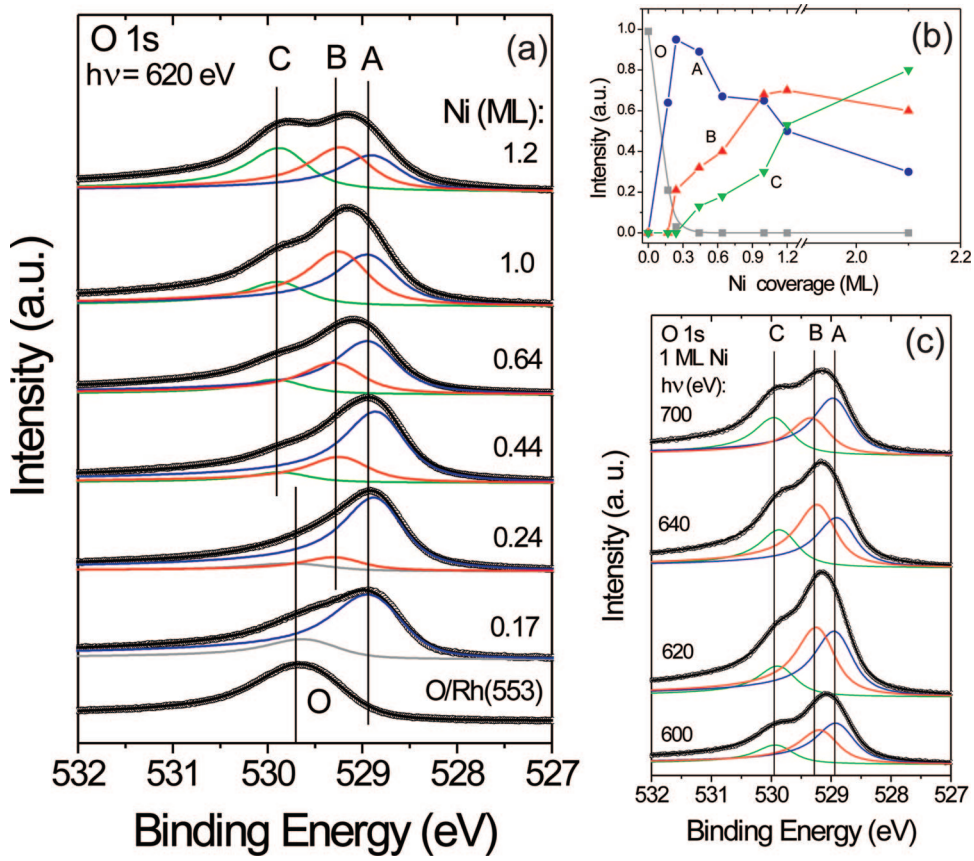

Figure 7. (a) O1s XPS spectra of Rh(553) exposed to 50 L oxygen and covered with various amounts of Ni followed by saturation exposure to O_2 ($h\nu = 620$ eV, normal emission); the nominal Ni coverages are indicated. The decomposition analysis of the spectra into O, A, B, and C spectral components is discussed in the text. (b) Intensity of O, A, B, and C components as a function of Ni coverage. (c) O 1s XPS spectra of 1 ML Ni oxidized as a function of photon energy (normal emission); $h\nu = 600-700$ eV.

edge) spectrum of the 0.44 ML Ni−O/Rh(553) surface. For comparison, the L-edge NEXAFS spectrum of bulk NiO, obtained from a 12 ML epitaxial film of NiO(100) on Pd(100), is included in Figure 8. The spectrum of the 0.44 ML Ni−O on Rh(553) surface displays two relatively simple structures at the L_3 and L_2 edges at ~853 and ~869 eV photon energy, respectively. This spectrum is very different from the corresponding spectrum of bulk-type NiO(100) and thus confirms the novel character of the Ni−O−Rh hybrid structures. The NEXAFS spectra of the Ni−O−Rh structures show clear dichroic effects as a function of the direction of the linearly polarized photon beam, with a peak energy shift of about −0.8 eV at the L_3 edge when going from normal (90°) to grazing incidence (20°) (data not shown). This is similar to what has been observed by Haverkort et al. [22] for 1 ML NiO(100) on Ag(100) and by Agnoli et al. [23] for the c(4 × 2) Ni_3O_4 monolayer structure on Pd(100), indicating the absence of octahedral Ni−O coordination spheres in accordance with the structural models discussed above.

Finally, an interesting topic concerns the oxidation kinetics of the Ni-decorated stepped Rh surfaces. In our previous work, it has been reported that the monatomic 1D Ni nanowires formed on Rh(553) at a Ni coverage of 0.2 ML display a significantly enhanced reactivity toward selective oxidation as compared to the bare Rh surface.[7] Here we expand this study and investigate the reactivity of the Ni nanostructures for various Ni coverages, keeping in mind the bimetallic aspects of the Ni−Rh line structures (i.e., considering only low Ni coverages). Figure 9 is a plot of the O 1s intensity as a function of the oxygen dose (in Langmuir) for different Ni coverages, representing the oxygen

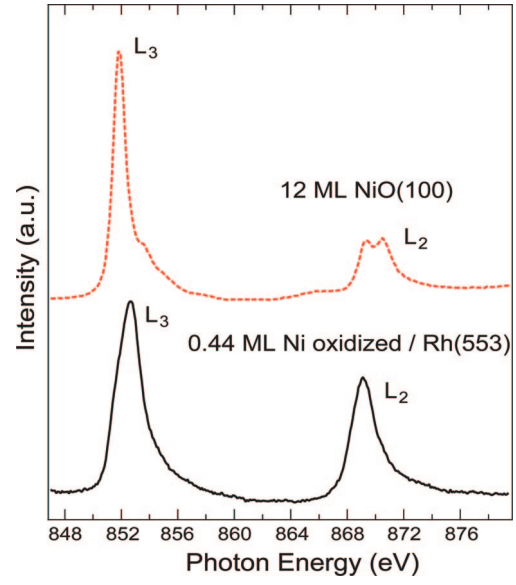

Figure 8. L-edge NEXAFS spectrum of 0.44 ML Ni−O taken at normal incidence (lower curve). Corresponding spectrum for 12 ML NiO(100) grown on Pd(100) (upper curve).

uptake kinetics, or, related to it, the reactivity of the various systems. On Rh(553) the oxygen uptake is fast for 0.1 and 0.2 ML Ni coverages where a saturation is reached at ~3−4 L O_2, whereas on the 0.4 ML Ni/Rh(553) surface the oxygen uptake is significantly slower and saturation is not even reached after 10−12 L O_2. This result confirms our previous findings and emphasizes the particularly high reactivity of the monatomic

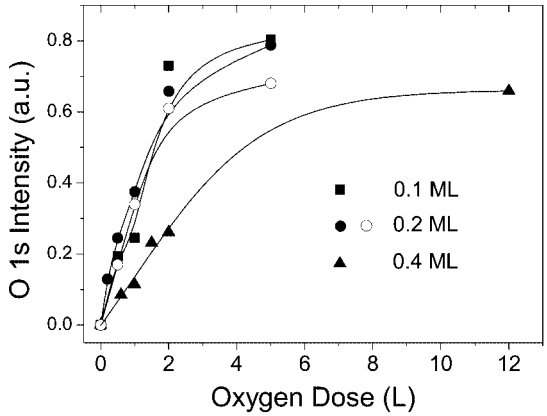

Figure 9. Total O 1s intensity versus O_2 dose for 0.1 ML Ni (filled squares), 0.2 ML Ni (filled circles), and 0.4 ML Ni (filled triangles) on Rh(553). Open circles correspond to 0.2 ML Ni on Rh(15 15 13). Solid lines are drawn as a guide for the eye.

quasi-1D bimetallic Ni−Rh nanowires toward oxygen; it has been explained on the basis of DFT calculations by the coupling of Ni and Rh d-states and the concomitant modifications of the local d-band center position.[7] For the higher Ni coverage, this effect becomes less significant, since the Ni atoms now forming the steps are not directly coupled to the Rh step atoms any more. In Figure 9, data obtained on the 0.2 ML Ni-decorated Rh(15 15 13) surface have also been included for comparison. They show that the reactivities of the Ni-decorated Rh(553) and Rh(15 15 13) surfaces toward oxygen are quite comparable, confirming the expectation of the local character of step-induced effects on the chemical reactivity of surfaces.

4. Conclusions

The growth of Ni nanostructures on vicinal Rh(111) surfaces and their oxidation have been investigated by STM, LEED, work function measurements, and X-ray core level spectroscopies. The Ni adatoms first decorate the Rh step edges at low coverages forming quasi-1D line structures and grow in a pseudomorphic layer-by-layer mode subsequently, up to Ni coverages of ~2 ML. The platelet-type morphology of the Ni adlayer is determined by step-flow growth processes with a 1D Schwoebel-type diffusion barrier around kink sites. The LEED and work function measurements suggest that the Ni films relax to the Ni bulk structure between 5 and 10 ML; the step morphology of the substrate is imprinted onto the Ni films up to at least 5 ML. The oxidation of the Ni-decorated stepped Rh surfaces lead to uniaxially ordered Ni−O (2 × 1) and (6 × 1) monolayer structures; the oxidized Ni surfaces converge to local NiO (100)-type and (111)-type reconstructions at higher coverages (≥2 ML). The O 1s XPS spectra reveal three chemically different O species in the 2D adlayers, which according to NEXAFS are different from bulk-type NiO and represent distinct nanolayer phases. The quasi-1D bimetallic Ni−Rh line structures at low coverage display the highest chemical reactivity toward oxygen from the gas phase.

Acknowledgment. This work has been supported by the Austrian Science Funds within the National Research Network "Nanoscience on Surfaces". F.P.N. acknowledges with gratitude the excellent hospitalities of Professor Wolf-Dieter Schneider, EPFL Lausanne, and Professor Charlie Campbell, University of Washington, during his sabbatical stays in Lausanne and Seattle in 2008.

References and Notes

(1) Sinfeld, J. H. *Bimetallic Catalysts: Discoveries, Concepts and Applications*; Wiley: New York, 1983.
(2) Campbell, C. T. *Annu. Rev. Phys. Chem.* **1990**, *41*, 775.
(3) Sachtler, W. M. H.; Somorjai, G. A. *J. Catal.* **1983**, *81*, 77.
(4) Hoster, H. E.; Bergbreiter, A.; Erne, P. M.; Hager, T.; Rauscher, H.; Behm, R. J. *Phys. Chem. Chem. Phys.* **2008**, *10*, 1.
(5) Chen, D. A.; Friend, C. M. *J. Phys. Chem. B* **1998**, *102*, 106.
(6) Schoiswohl, J.; Mittendorfer, F.; Surnev, S.; Ramsey, M. G.; Andersen, J. N.; Netzer, F. P. *Surf. Sci.* **2006**, *600*, L274.
(7) Schoiswohl, J.; Mittendorfer, F.; Surnev, S.; Ramsey, M. G.; Andersen, J. N.; Netzer, F. P. *Phys. Rev. Lett.* **2006**, *97*, 126102.
(8) Surnev, S.; Vitali, L.; Ramsey, M. G.; Netzer, F. P.; Kresse, G.; Hafner, J. *Phys. Rev. B* **2000**, *61*, 13945.
(9) Nyholm, R.; Andersen, J. N.; Johansson, U.; Jensen, B. N.; Lindau, I. *Nucl. Instrum. Methods Phys. Res., Sect. A* **2001**, *467−468*, 320.
(10) Ivanco, J.; Haber, T.; Krenn, J. R.; Netzer, F. P.; Resel, R.; Ramsey, M. G. *Surf. Sci.* **2007**, *601*, 178.
(11) Gambardella, P.; Kern, K. *Surf. Sci.* **2001**, *475*, L229.
(12) Himpsel, F. J.; Knapp, J. A.; Eastman, D. E. *Phys. Rev. B* **1979**, *19*, 2872.
(13) Fischer, N.; Schuppler, S.; Fauster, Th.; Steinmann, W. *Phys. Rev. B* **1990**, *42*, 9717.
(14) Pearl, T. P.; Darling, S. B.; Sibener, S. J. *Surf. Sci.* **2001**, *491*, 140.
(15) Hildebrandt, S.; Hagendorf, Ch.; Doege, T.; Jeckstiess, Ch.; Kulla, R.; Neddermeyer, H. *J. Vac. Sci. Technol., A* **2000**, *18*, 1010.
(16) Hagendorf, Ch.; Shantyr, R.; Neddermeyer, H.; Widdra, W. *Phys. Chem. Chem. Phys.* **2006**, *8*, 1575.
(17) Parteder, G; Surnev, S. Netzer, F. P. Unpublished data.
(18) Barbier, A.; Mocuta, C.; Kuhlenbeck, H.; Peters, K. F.; Richter, B.; Renaud, G. *Phys. Rev. Lett.* **2000**, *84*, 2897.
(19) Wander, A.; Bush, J. J.; Harrison, N. M. *Phys. Rev. B* **2003**, *68*, 233405.
(20) Wagner, M. Diploma Thesis, Karl-Franzens University, Graz, June 2008.
(21) de Groot, F. M. F. *J. Electron Spectrosc. Relat. Phenom.* **1994**, *67*, 529.
(22) Haverkort, M. W.; Csiszar, S. I.; Hu, Z.; Altieri, S.; Tanaka, A.; Hsieh, H. H.; Lin, H.-J.; Chen, C. T.; Hibma, T.; Tjeng, L. H. *Phys. Rev. B* **2004**, *69*, 020408(R).
(23) Agnoli, S.; Sedona, F.; Finetti, P.; Rizzi, G. A.; Granozzi, G.; Bondino, F.; Zacchigna, M.; Parmigiani, F. *J. Phys. Chem. C* **2008**, *112*, 5123.

JP807259N